

Film-forming properties of estolides[†]

G. Biresaw^{a,*}, S. C. Cermak^b and T. A. Isbell^b

^aCereal Products and Food Science Research Unit, National Center for Agricultural Utilization Research, Agricultural Research Service, United States Department of Agriculture, 1815 N. University Street, Peoria, IL, 61604, USA

^bNew Crops and Processing Technology Research Unit, National Center for Agricultural Utilization Research, Agricultural Research Service, United States Department of Agriculture, 1815 N. University Street, Peoria, IL, 61604, USA

Received 29 August 2006; accepted 5 February 2007; published online 8 March 2007

Estolides are biobased materials obtained from the synthesis of ingredients derived from agricultural products. They are oligoesters obtained by the reaction of fatty acids and/or methyl esters with a double bond. By varying the chemistries of the starting materials and the reaction conditions, estolides of varying chemical structures (e.g., branching), and physical properties (e.g., mol wt, viscosity, pour point, cloud point) are obtained. Estolides have been found to have suitable properties for some lubrication applications. In this work, the effect of estolide physical/chemical variability on film thickness and pressure–viscosity coefficient (pvc) were examined. The results showed that estolides have lower pvc than the non-polar hydrocarbon PAO, but much higher than seed oils (e.g., soybean, jojoba, canola), which are used as feedstock in estolide synthesis. The film thickness and pvc properties of estolides were also found to be dependent on the structure (e.g., homo- versus co-oligomer) and purity of the estolide oils.

KEY WORDS: biodegradable oils, biobased oils, EHL, estolides, film thickness, polyalphaolefin, pressure–viscosity coefficient, vegetable oils

1. Introduction

Biobased materials are those manufactured using feedstocks generated from plants and/or animals [1]. They differ from petroleum-based materials in that they have unlimited and renewable raw material base. Examples of such raw materials include agricultural products such as starches, proteins, fats, and oils. Application of these agriculture-based raw materials in the manufacture of biobased products occurs through various routes. The most preferred route is that of applying the ag-based raw materials, with little or no additional processing, in biobased manufacture. However, manufacture of comparable products through simple replacement of petroleum-based ingredients with biobased ingredients is not possible. For many applications, biobased raw materials require further processing (chemical, physical, enzymatic, etc.) to make them suitable for biobased material manufacture. Such processing, which may be simple or extensive, will impact the cost of biobased product manufacture, and its competitiveness to petroleum-based products.

Various degrees of further processing of ag-based raw materials is employed in the development of biobased

lubricants. In some cases, various additives are used to enhance the properties of ag-based raw materials so that its performance is comparable to those of petroleum-based lubricants. This approach is extensively used in the development of biobased lubricants from seed oils [2]. In other cases, ag-based raw materials and/or its derivatives are used as feedstocks in biobased lubricant development. The latter approach is applied in the generation of estolides in biobased lubricant development.

Estolides are obtained from the synthesis of ingredients derived from agricultural products [3]. They are oligoesters obtained by the reaction of fatty acids and/or methyl esters with a double bond. The simplest estolide synthesis involves a reaction between two identical molecules comprising both fatty acid and double bond, to produce a homo-oligomer estolide. Co-oligomer estolides are obtained by the reaction of two different molecules, one of which has the fatty acid and the other the double bond. In almost all cases, the synthesis of estolides involves esterification of the terminal free fatty acid of the estolide with an alcohol such as 2-ethylhexyl alcohol.

The chemistries of estolides can be varied through various means including: changing the fatty acids or esters used to react with the estolide bond, changing the alcohols used to esterify the terminal free fatty acid, changing the reaction conditions (time, temperature, catalyst, stirring and mixing rate) to vary the degree of oligomerization, etc. Thus, by varying the chemistries of

[†]Names are necessary to report factually on available data; however, the USDA neither guarantees nor warrants the standard of the product, and the use of the name by the USDA implies no approval of the product to the exclusion of others that may also be suitable.

*To whom correspondence should be addressed.

E-mail: biresawg@ncaur.usda.gov

the starting materials and the reaction conditions, one can synthesize estolides with desired polarity, chemical structure (e.g., branching), and physical properties (e.g., mol wt, viscosity, pour point, cloud point). This provides a powerful tool for producing biobased fluids with the required characteristics for the needed tribological process. Estolides are biobased since the saturated and unsaturated fatty acids used in its synthesis are obtained from ag-based fats and oils.

Over the years, various physical properties of estolides of interest in lubricant application have been investigated. These include: viscosity, viscosity index, pour point, cloud point, iodine value, acid value, Gardner color, oxidation stability, etc [3–8]. These studies indicated that estolides have suitable properties for some lubrication applications. However, the effect of estolide chemical/physical characteristics on its tribological properties have yet to be fully understood. Most tribological processes occur in one of three regimes: boundary, hydrodynamic, and mixed lubrication regimes [9]. The film-forming properties of lubricants are critical in lubrications occurring in hydrodynamic and mixed-film regimes. These lubrication regimes are critical to a number of lubrication applications including metalworking, hydraulics, gear oils, etc.

Previous investigations into the tribological properties of biobased materials from our group included studying the effect of lubricant chemistry on its adsorption properties [10–14]. In these investigations, the adsorption of biobased oils, including seed oils of various chemical structures, from a non-polar base oil onto a polar surface is determined using boundary friction or interfacial measurements. The data is then used to construct an adsorption isotherm, which is analyzed using appropriate adsorption models. From such analysis, the free energy of adsorption, ΔG_{ads} , of the biobased oil is determined. Results from such studies showed that triglyceride seed oils such as soybean oil adsorb stronger than monoglyceride seed oils such as jojoba. These studies also showed that such structural differences as degree of unsaturation have minor effect on ΔG_{ads} .

In the work described here, estolide of varying physical/chemical properties are investigated for its film-forming properties. Homo- and co-oligomer estolides of varying degree of oligomerization are investigated and their film-forming properties compared to other synthetic and biobased fluids. In addition, the effect of side reaction products on the film-forming properties of estolides are examined.

2. Experimental

2.1. Materials

Polyalphaolefin oil (PAO), was a commercial sample (Durasyn 166) supplied by BP Amoco (Naperville, IL)

and used as supplied. The estolides used in this work were synthesized as described below. The following materials were used in the synthesis of the estolides: perchloric acid (70%) and 2-ethylhexyl alcohol were purchased from Fisher Scientific Co. (Fairlawn, NJ); potassium hydroxide was obtained from J. T. Baker Chemical Co. (Phillipsburg, NJ); filter paper was obtained from Whatman (Clifton, NJ); ethanol was purchased from AAPER Alcohol and Chemical Company (Shelbyville, KY); fatty acid methyl ester (FAME) standard mixtures were obtained from Alltech Associates, Inc. (Deerfield, IL).

Isopropyl alcohol (99+%), and hexanes (99+%) used for cleaning the film thickness measurement instrument and specimen were obtained from Aldrich Chemical Company, Milwaukee, WI, and used as supplied.

2.2. Synthesis of oleic (EST-O) and coco-oleic (EST-CO) estolide esters

EST-O is a homo-oligomer estolide obtained by the self-condensation of oleic acid. EST-CO is a co-oligomer estolide and is obtained by the reaction of the carboxylic group of coconut acid (mainly lauric acid) with the double bond of oleic acid. Schematic of the procedure for the synthesis of EST-O and EST-CO, as well as the structures of the reactants and products are shown in figure 1. As shown in figure 1, the procedure yields significant quantities of side products, which are removed by distillation. Thus, the purity of the estolides is highly dependent on the quality of the distillation process. Another characteristics of this synthesis procedure is that the estolide produced comprises mixtures of oligomers with varying degrees of oligomerization ($n = 0-6$ for EST-O, $n = 0-9$ for EST-CO). Details on the synthesis and purification of the estolides can be found elsewhere [7,15].

2.3. Characterization of estolide esters

Estolides were characterized before and after purification, and the results are summarized in tables 1, 2. Brief description of the characterization procedures are given next.

2.3.1. Purity and oligomer distribution

The estolide number (EN) was determined by gas chromatography (GC). Estolide samples had to be esterified as described before [3] prior to GC injection. GC analysis was performed with a Hewlett-Packard 6890 Series gas chromatograph (Palo Alto, CA) equipped with a flame-ionization detector and an autosampler/injector. Analyses were conducted on a SP-2380 30 m \times 0.25 mm i.d. column (Supelco, Bellefonte, PA). Parameters for SP-2380 analysis were: column flow

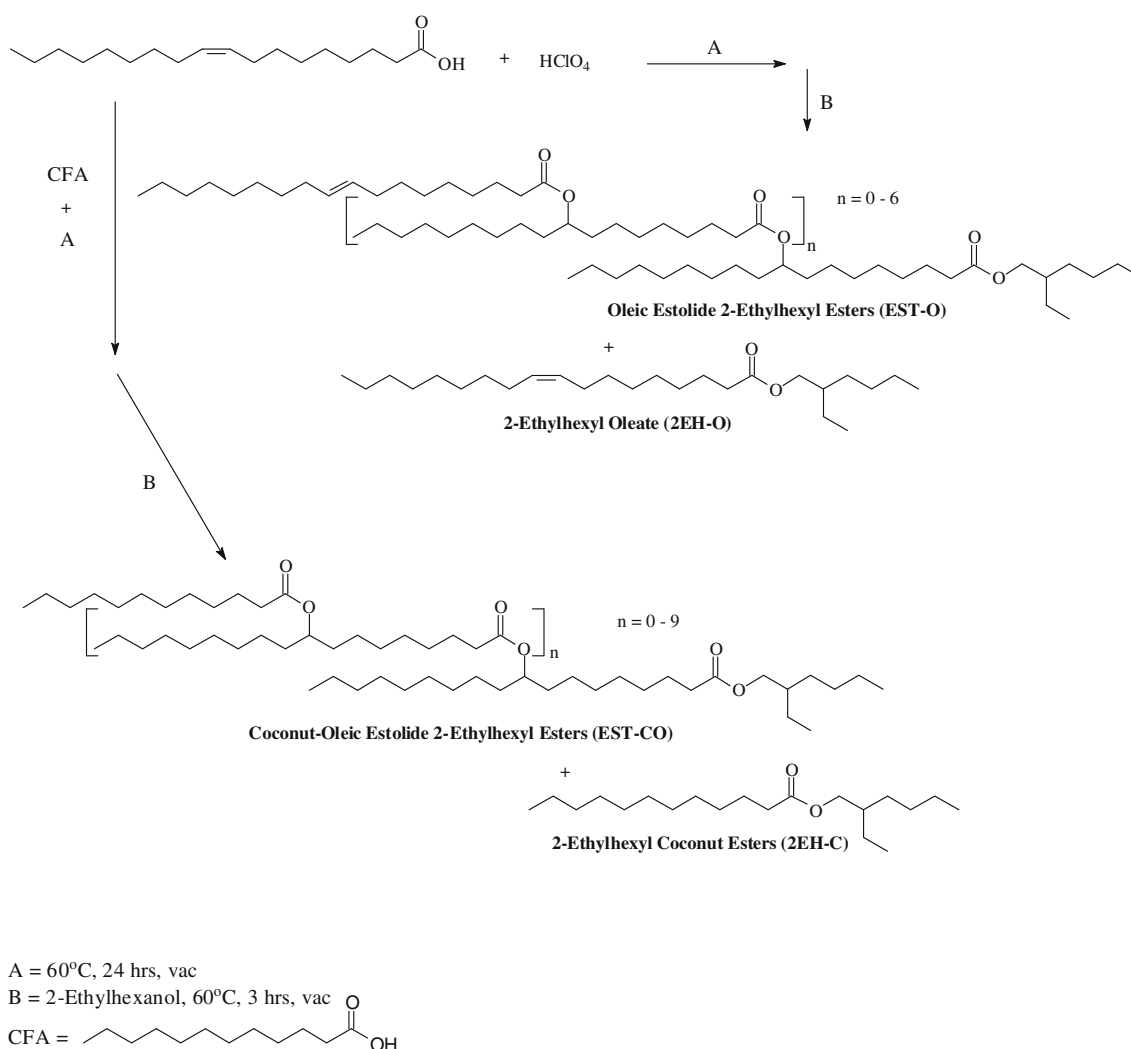


Figure 1. Schematics of the synthesis of oleic (EST-O) and coco oleic (EST-CO) estolide esters.

1.4 mL/min with helium head pressure of 20 psi; split ratio 10:1; 120–165 °C at 10 °C/min, 165–175 °C at 3 °C/min, 175–265 °C at 10 °C/min, hold 5 min at 265 °C; injector and detector temperatures set at 250 °C.

The ENs were determined based on the percent hydroxy in the sample. The oligomerization was further explored by HPLC. Reverse phase HPLC analyses were performed on a Thermo Separations Spectra System AS1000 autosampler/injector (Fremont, CA) with a P2000 binary gradient pump from Thermo Separation Products (Fremont, CA) coupled to an Alltech ELSD 500 evaporative light scattering detector (Alltech Associates, Deerfield, IL). A C-8 reverse phase analysis used to separate reaction mixtures was carried out with a Dynamax column (250 mm × 4.5 mm, 8 μm particle size) from Rainin Instrument Co. (Woburn, MA). Components were eluted at a flow rate of 1 mL/min; 0–2 min 60% acetonitrile 40% acetone; 20–25 min 100% acetone; 30–35 min 60% acetonitrile 40% acetone. The ELSD drift tube was set at 55 °C with the nebulizer set at 20 psi N₂, providing a flow rate of 2.0 standard liters

per minute (SLPM). Retention times for eluted peaks were: estolides esters, 13.2–23.8 min and 2-ethylhexyl oleate 8.8 min.

2.3.2. Dynamic viscosity

Dynamic viscosity was measured on AR2000 controlled-stress rheometer (SN 3F2300) using the double concentric cylinders fixture (TA Instruments – Waters LLC, New Castle, DE). The instrument is equipped with version 5.2 firmware, and TA Instruments Advantage software version 4.3 (TA Instruments – Waters LLC, New Castle, DE). Viscosity was measured at 40 and 100 °C as a function of shear rate, which was varied from 100 to 10 s⁻¹. The instrument is equipped with a Peltier Plate heating/cooling system (TA Instruments – Waters LLC, New Castle, DE), capable of temperature control in the range –30 to 180 °C.

2.3.3. Kinematic viscosity

Kinematic viscosity was measured using calibrated Cannon-Fenske viscometer tubes (Cannon Instrument

Table 1.
Properties of fluids synthesized in this work

Oil ID	Oil description	Non-EST (a) (%)	EST Total (%)	Estolide oligomer composition			
				Mono (%)	Di (%)	Tri (%)	4+ (%)
EST-O	Distilled oleic estolide	4.7 (b)	95.3	37.3	25.2	16.4	17.4
EST-O-U	Undistilled oleic estolide	28 (b)	72	–	–	–	–
2EH-O	2-Ethylhexyl oleate	>97 (b)	<3	–	–	–	–
EST-CO	Distilled coco oleic estolide	<1 (c)	>99	43.2	28.1	14.1	14
PAO	Polyalphaolefin (D166)						

(a) Amount of non-estolide in the oil.(b) 2-Ethylhexyl oleate.(c) 2-Ethylhexyl coconut ester.

Table 2.
Some physical properties of oils (a)

Oil ID	CP (°C)	PP (°C)	dVisc (cP)		kVisc (cSt)		VI	EN	Ref
			40 °C	100 °C	40 °C	100 °C			
			EST-O	–37	–33	76.5 ± 0.4			
EST-CO	–35	–33	55.3 ± 0.3	9.5 ± 0.1	72.18	12.70	177	1.45	b
EST-O-U	–24	–30	34.8 ± 0.2	6.10 ± 0.03	39.62	8.29	192	0.75	b
PAO			24.4 ± 0.2	4.4	31.0	5.9	138	–	c
2EH-O	–15	–30	9.11 ± 0.07	2.54 ± 0.05	10.70	3.09	161	0.065	b

(a) Methods: CP, cloud point; PP, pour point; dVisc, dynamic viscosity; kVisc, kinematic viscosity; VI, viscosity index; EN, estolide number.(b) This work.(c) Ref [16].

Co., State College, PA), in a Temp-Trol (Precision Scientific, Chicago, IL) viscometer bath set at 40.0 and 100.0 °C. Viscosity and viscosity index were calculated using ASTM D 445-97 and D2270-93 methods, respectively. All viscosity measurements were run in duplicate and the average values are reported.

2.3.4. Pour point

Pour point is defined as the coldest temperature at which the sample still poured, and was measured following ASTM D97-96a method to an accuracy of ±3 °C. All pour points measurements were run in duplicate and average values are reported.

2.3.5. Cloud point

Cloud point was determined using ASTM D2500-99 method to an accuracy of ±1 °C. Duplicate measurement of cloud point were conducted and average values are reported.

2.4. Film thickness measurement

Lubricant film thickness was measured by optical interferometry between a glass disc and steel ball on an EHL Ultra Thin Film Measurement System (PCS Instruments, London, England). The disk used in film thickness measurement is 100 mm diameter by 12 mm thick float glass, coated with about 20 nm semi-reflecting chrome layer, which in turn is coated with ~500 nm thick silica spacer layer. The ball is a super finished 3/4" diameter, G10 carbon Cr steel (AISI 52100) precision

steel ball. Other pertinent specifications of the instrument are as follows: measured film thickness, 1–1000 ± 1 nm; rolling speed, 0–5 m/s; slide-to-roll ratio, 0–200%; applied load, 0–50 N; maximum steel/glass contact pressure of 0.7 GPa; lubricant temperature range, ambient to 150 °C. Film thickness was measured at various combinations of speed, load, and temperature, which were varied as follows: speed, 0.02–3.0 m/s in 20% increments; load, 10–40 N in 10 N increments; temperature, 30, 40, 70, 100, and 120 °C. Film thickness data was analyzed using IgorPro Vesion 5.0.3.0 software (WaveMetrics, Inc., Lake Oswego, OR). Details on the application of interferometry for lubricant film thickness measurements can be found elsewhere [17]. Detailed description of the EHL Ultra Thin Film Measurement System and test procedure has been given before [16].

3. Results and discussion

3.1. Properties of the oils investigated

In this work, the film thickness properties of five oils, including a homo-oligomer and a co-oligomer estolide, were investigated. Of the five oils, four were products from estolide synthesis conducted in this work. The fifth was polyalphaolefin (PAO), a commercial synthetic hydrocarbon oil. These oils are listed in table 1, which also shows some of their characteristics along with the designations that will be used to refer to each of the oils henceforth in this manuscript.

As shown in table 1, the four oils obtained from estolide synthesis had different degrees of purity. Three

of these oils, EST-O, EST-O-U, and 2EH-O were obtained from the synthesis of the homo-oligomer oleic estolide. EST-O is the residue estolide obtained after the distillation of the oleic estolide reaction product mixture, and contains 4.7% of the by-product 2-ethylhexyl oleate (2EH-O). EST-O-U is the oleic estolide reaction product mixture that was not subjected to the distillation process, and contains 28% of 2EH-O. The third oil is 2EH-O, the distillate of the reaction product mixture from oleic estolide ester synthesis, and contains less than 3% of oleic estolide ester. The fourth oil, EST-CO, is the residue from the distillation of the co-oligomer coco-oleic estolide ester reaction product mixture. EST-CO contains more than 99% coco-oleic estolide ester, and less than 1% of the reaction by-product 2-ethylhexyl coconut ester.

Table 1 also shows the concentrations of oligomers of varying degree of oligomerization in the distilled estolides ester. Table 2 is a summary of some physical properties of the oils, including their kinematic and dynamic viscosities.

3.2. Effect of measurement parameters on estolide film thickness

Film thickness was measured as a function of entrainment speed, at various loads and temperatures. Entrainment speed, u , is defined as follows

$$u = (u_1 + u_2)/2, \quad (1)$$

where u_1 , u_2 are the speeds of the disk and ball in m/s.

All measurements were conducted under pure rolling conditions, i.e., at slide-to-roll ratio (SRR) of 0%. SRR is defined as follows

$$\text{SRR} = |u_1 - u_2|/u = (2|u_1 - u_2|)/(u_1 + u_2). \quad (2)$$

All fluids displayed similar film thickness behavior with varying entrainment speed u . This is illustrated in figure 2, which shows the effects of temperature and speed on the film thickness of EST-CO at 20 N load. As shown in figure 2, regardless of the temperature, decreasing entrainment speed caused a linear decrease in film thickness. The data in figure 2 also shows another feature common to all the fluids investigated, which is that the film thickness increased with decreasing temperature. This is attributed to the effect of temperature on viscosity. Decreasing temperature will result in higher viscosity and thicker lubricant film. Both of these features are consistent with the EHL theory [18] as described by equation (3)

$$h = k(u\eta)^{0.67} \alpha^{0.53}, \quad (3)$$

where h is the lubricant film thickness (nm), k is a constant dependent on test geometry; η is dynamic viscosity at ambient atmospheric pressure (cP), and α is pressure-viscosity coefficient (GPa^{-1}) at the test temperature.

The data in figure 2, especially those at lower temperatures can be adequately predicted using equation (3). This is illustrated in figure 2 by the fit of the data generated at 40 °C, which gave a slope of 0.69 ± 0.02 , which is within the range of the theoretical value of 0.67 given in equation (3). However, at higher temperatures (≥ 70 °C), the film thickness displayed significant deviations from linearity below a speed of about 0.15 m/s.

The effect of load and speed on film thickness is illustrated in figure 3, which shows measurements at 40 and 100 °C on coco oleic estolide ester [EST-CO]. The data in figure 3 shows that film thickness is independent of load, at almost all entrainment speeds and temperatures. This

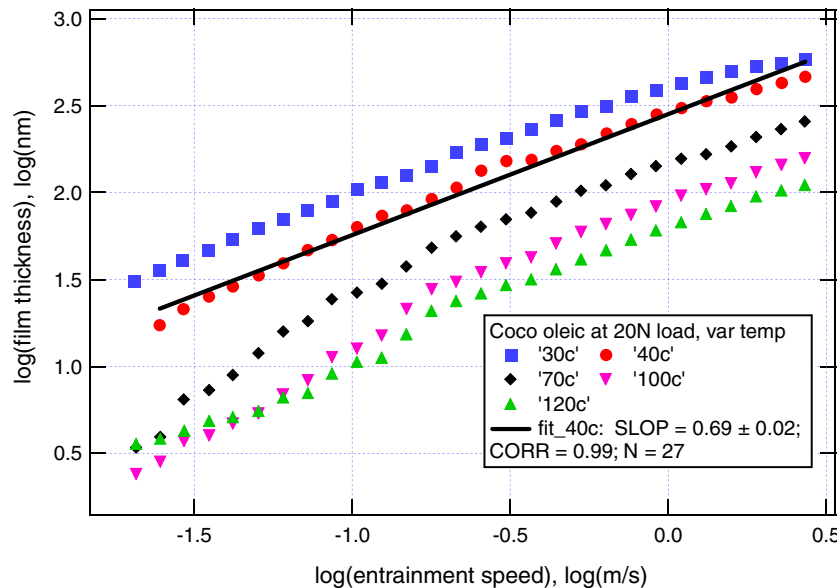


Figure 2. Effect of temperature and speed on the film thickness of coco oleic estolide ester.

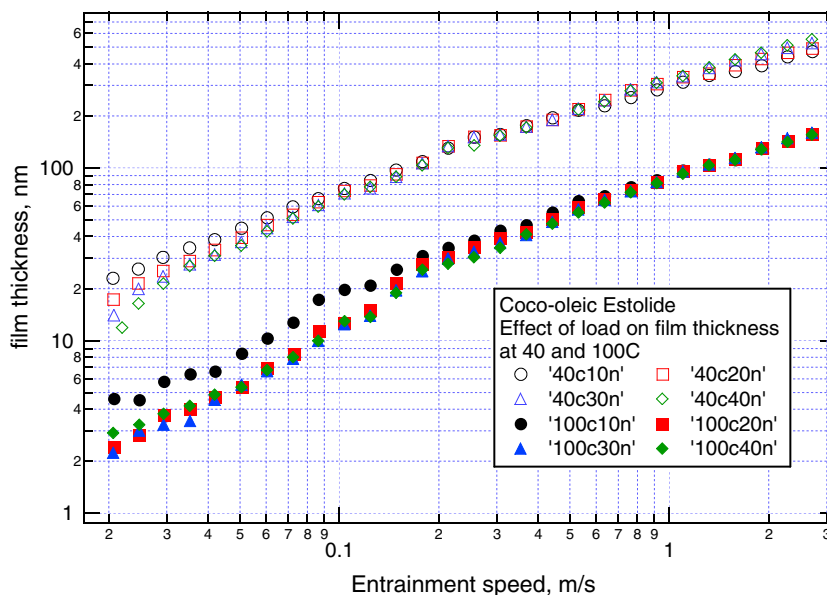


Figure 3. Effect of load and speed on the film thickness of coco oleic estolide ester at 40 and 100 °C.

observation is common to all the fluids investigated in this work. A minor dependence of film thickness on load was observed at very low speeds and/or very high temperatures.

3.3. Effect of lubricant properties on film thickness

Figure 4 compares the film thickness of the five oils as a function of entrainment speed at 100 °C and 40 N load. The points in figure 4 are the measured film thickness values (h_m) and the lines are those calculated (h_c) using a equation (3). As shown in figure 4, the measured film thickness of the estolide esters display two

regions of film thickness: linear and non-linear. At high speeds, h_m shows a linear decrease with decreasing speed, and the values for the different oils have similar slopes and are parallel. However, below a certain critical speed, h_m values deviate from the linear trend and continuously decrease with decreasing entrainment speed. The speed at which transition of h_m from linear to non-linear occur varies from oil to oil, and appears to be a function of the estolide viscosity. Thus, the low viscosity 2EH-O deviated from the linear trend at a much higher entrainment speed than the more viscous estolide esters.

Examination of the h_m values at the high entrainment speed region indicates that the values for the different estolide oils follow their relative viscosities. Thus,

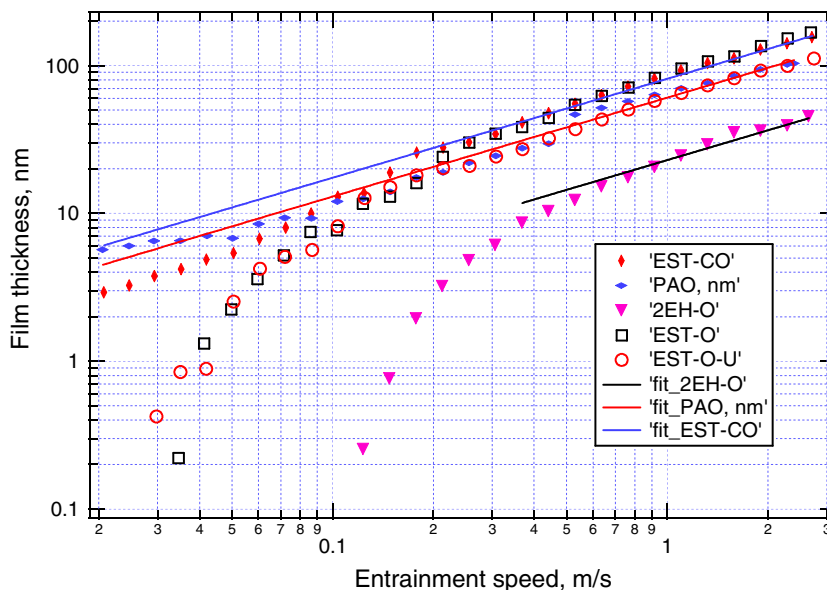


Figure 4. Effect of estolide chemistry on film thickness at 100 °C and 40 N load.

2EH-O, which had the lowest viscosity of the estolides at 100 °C (table 2) gave the thinnest film, whereas EST-O which had the highest viscosity of the estolides gives the thickest film. Examination of figure 4 also shows that PAO which has lower viscosity than EST-O-U (table 2), gave comparable film thickness to EST-O-U. This discrepancy between relative viscosities and film thickness of PAO versus EST-O-U might be a reflection of the difference in the chemical structures between the two oils. PAO is a non-polar hydrocarbon whereas EST-O-U is a polar oligo-ester. It appears that the non-polar hydrocarbons generally give higher film thickness than polar oils. This difference in chemical structure might be reflected in differences in pressure–viscosity coefficient (pvc), which will have an effect on film thickness (equation 3). Despite the discrepancy between PAO and EST-O-U, linear regression analysis of $\log(\eta)$ versus $\log(h)$ data from all five oils, at all combinations of two temperatures (40, 100 °C), four loads (10, 20, 30, 40 N), and 1.1 m/s, which is in the high entrainment speed region, gave a slope of 0.70 ± 0.4 (CORR = 0.99), which is in the range predicted by equation (3).

In general, calculated (h_c) versus measured (h_m) film thickness of lubricants in the low speed region display three types of trends [19,20]: positive deviation, i.e., $h_m > h_c$; negative deviation, i.e., $h_m < h_c$; and no deviation, i.e., $h_m = h_c$. Examination of figure 4 in the low speed region shows that at 100 °C and 40 N, all the estolides displayed negative deviations, whereas PAO displayed slight or no deviation. Comparing the estolides to each other, it is clear that, even though they all showed negative deviations, the relative deviations were different. Table 3 compares h_m versus h_c of PAO and the estolide esters displayed in figure 4 at 0.05 m/s, which is in the low speed region. At this speed, the measured film thickness does not correlate at all with the viscosities of the oils as predicted by equation (3). This is a major contrast with the observation at 1.1 m/s in the high speed region (data not given here). Thus, in the low speed region, PAO, which has the lowest viscosity, gave the thickest film whereas EST-O which has the highest viscosity gave the thinnest measured film (table 3). PAO also gave the smallest negative deviation of all the oils. As mentioned before, the difference between PAO and the rest of the oils is that PAO is non-polar, whereas the

rest of the oils are polar, and this might explain the difference in the film-forming properties of PAO versus the estolide esters.

The data in table 3 also shows that, in the low speed region, EST-CO gave a thicker film than EST-O, even though EST-CO has lower viscosity than that of EST-O. As a result, EST-CO showed a significantly smaller negative deviation than EST-O. The main difference between these two oils is their chemical structure in that EST-CO is a co-oligomer of two different fatty acids, (oleic and coconut acids), whereas EST-O is a homo-oligomer of oleic acid. It appears that co-oligomerization leads to thicker film than homo-oligomerization, even at relatively lower viscosity. In addition, it should be noted that EST-CO has a slightly higher purity and EN than EST-O, which might also contribute to the larger film thickness of EST-CO.

The data in table 3 and figure 4 also show that, in the low speed region, EST-O-U and EST-O displayed similar measured film thicknesses. These two oils have similar chemical structures but differ in their purities and viscosities. Since EST-O has a higher h_c value, it also displayed a larger negative deviation than EST-O-U. One way of explaining the fact that the difference in the degree of purity between EST-O and EST-O-U did not affect their respective h_m values in the low speed region is to invoke the concept of fractionation [19–23]. According to this concept, at low entrainment speeds, highly polar species preferentially fractionate from the bulk and adsorb on the friction surfaces, and the film thickness is a function of the viscosity of these highly polar species and not that of the bulk fluid. Application of this concept to the present result implies that the same chemical species is responsible for the film thickness of EST-O and EST-O-U. Moreover, this chemical species, in addition to being more polar than the bulk, must also be less viscous than the bulk, since it resulted in negative deviation, i.e., $h_m < h_c$. Fractionation has been proposed to explain phenomenon in which measured film thickness showed positive or negative deviations from the calculated value [19–23]. The structure of the low viscosity and highly polar species which might be responsible for the observed negative deviations in EST-O and EST-O-U has yet to be identified.

Table 3.

Effect of chemical structure on measured (h_m) versus calculated (h_c) film thickness of oils in the low entrainment speed region (0.05 m/s), 100 °C, and 40 N load

Oil	Polar	Purity (%)	Oligomer type	EN	u (m/s)	dVis (cP)	h_m (nm)	h_c (nm)	$h_m - h_c$ (nm)
PAO	No	100	N/A	N/A	0.05	4.4	6.7	8.2	-1.5
EST-O-U	Yes	72	Homo	0.75	0.05	6.1	2.5	7.8	-5.3
EST-CO	Yes	>97	Co	1.45	0.05	9.5	5.3	10.9	-5.6
EST-O	Yes	95.3	Homo	1.27	0.05	11.8	2.2	11.4	-9.2

3.4. Pressure–viscosity coefficient of estolides

Pressure–viscosity coefficient (pvc) of a test fluid can be determined from film thickness data using equation (3) [24]. The procedure for pvc determination using this method requires film thickness data for a fluid with known pvc data, which will be referred to as the reference fluid, under identical conditions as that of the test fluids. The pvc for the test fluid is then obtained by combining equation (3) for the test and reference fluids, and solving it for the pvc of the test fluid as follows

$$\alpha_t = \alpha_r [(h_t/h_r)(a_r/a_t)]^{[1/0.53]}, \quad (4)$$

where α_t , α_r are, respectively, the pvc of test and reference fluids; h_t , h_r are, respectively, the film thickness of the test and reference fluids under identical test conditions; a_t , a_r are the corresponding viscosity–speed parameters defined as follows

$$a_t = (u_t \eta_t)^{0.67}; \quad a_r = (u_r \eta_r)^{0.67}, \quad (5)$$

where u_t , u_r are, respectively, the entrainment speeds of the test and reference fluids corresponding to h_t , h_r ; and, η_t , η_r are, respectively, dynamic viscosities of test and reference fluids at ambient atmospheric pressure and test temperatures.

In applying equations (4, 5) for determining the pvc of the estolides, we used PAO as the reference fluid since its pvc has already been reported [24]. The dynamic viscosities of PAO and the test fluids used in these calculations are summarized in table 2. Using film thickness data generated under identical conditions (40 °C and 10 N load) for PAO and the test fluids, the pvc of each fluid was calculated using equations (4, 5). Two methods were used to estimate the pvc of the test fluids from such calculations. In the first method (Method-1), pvc was

calculated for the entire range of entrainment speed used in film thickness measurement. A typical result from such analysis is shown in figure 5, which is a plot of film thickness versus pvc for 2EH-O. In general, such analysis gives calculated pvc values that remain constant with decreasing film thickness up to a certain value of film thickness. Depending on the nature of the fluid, the calculated pvc might decrease, increase or remain unchanged when the film thickness is reduced beyond this value. The data for 2EH-O shown in figure 5 shows that the calculated pvc values remained at a constant steady-state value until about 50 nm of film thickness, but decreased with decreasing film thickness below 50 nm. The pvc of the fluid is obtained by averaging the steady-state pvc values above 50 nm film thickness. The average and standard deviation pvc data for all the fluids obtained using Method-1 are summarized in table 4.

In the second method (Method-2), which is widely practiced by many groups, pvc is calculated at a single entrainment speed. In this work, film thickness data at 1.1 m/s was used to calculate the pvc of the test fluids. As shown in table 4, the two methods gave comparable pvc values. Of the two methods, however, Method-1 is preferred since it allows for the estimation of the standard deviations for the calculated pvc values.

The data in table 4 shows that all the estolides have lower pvc than PAO. It also shows that the two purified estolides, EST-O and EST-CO had the highest pvc values of the four estolides. Comparison of the two purified estolides shows that EST-CO has a higher pvc than EST-O. This explains why EST-CO, in spite of its relatively lower viscosity than EST-O, displayed a higher film thickness and less negative deviation in the low speed region (see table 3, and figure 4). Thus, it appears that co-oligomerization results in a higher pvc than homo-

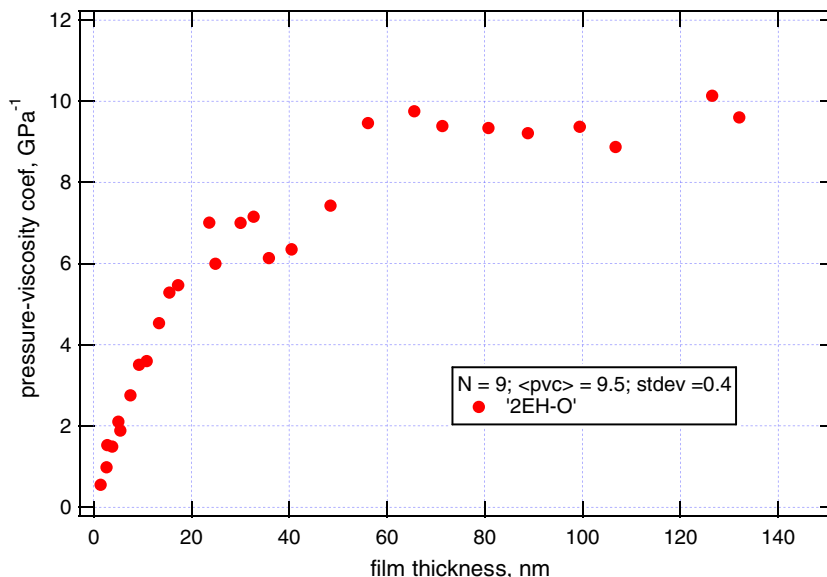


Figure 5. Effect of film thickness on pressure viscosity coefficient of 2EH-O.

Table 4.
Pressure–viscosity coefficient of estolide esters calculated from film thickness data at 40 °C and 10 N load

Oil	kVisc (cSt)	dVisc (cP)	Method-1 (a) (pvc) ± SD (Gpa ⁻¹)	Method-2 (b) pvc (Gpa ⁻¹)	Ref
PAO	31.0	24.4 ± 0.2	13.5	13.5	(c)
EST-O	87.9	76.5 ± 0.4	10.0 ± 0.7	10.2	This work
EST-CO	71.5	55.3 ± 0.3	12.0 ± 1.1	12.3	This work
EST-O-U	39.6	34.8 ± 0.2	9.2 ± 0.6	9.0	This work
2EH-O	10.7	9.11 ± 0.07	9.5 ± 0.4	9.3	This work
Canola		33.3 ± 0.2	10.0 ± 0.9		(d)
Soybean		30.3 ± 0.9	7.6 ± 0.9		(d)
Jojoba		21.2 ± 0.2	7.3 ± 0.5		(d)

(a) Calculated by averaging steady-state pvc values obtained from analysis of film thickness data in the entire entrainment speed range of the experiment (see figure 5).(b) Calculated using film thickness data at an entrainment speed of 1.1 m/s.(c) Ref [24].(d) Ref [16].

oligomerization. The reason why co-oligomerization favors higher pvc is a subject for future investigation.

The data in table 4 also shows that pvc is influenced by the purity of the oil mixture. Thus, EST-O, which has 4.7% residual 2EH-O, has a higher pvc than EST-O-U, which has 28% residual 2EH-O. In fact, the pvc of EST-O-U is similar to that of pure 2EH-O, which implies that 2EH-O dominates the film-forming property of EST-O-U. This implies that purification of estolide reaction mixtures will have a big impact on their film-forming properties.

Table 4 also compares the pvc values of seed oils estimated previously using Method-2 [16] with the fluids studied in this work. As can be seen in table 4, all the estolides have higher pvc values than soybean and jojoba oils; and comparable or higher pvc than canola oil. The purified estolides, specifically EST-CO, have substantially higher pvc than the seed oils. This comparison with seed oils is particularly interesting, since fatty acids from seed oils are used as feedstocks in estolide synthesis. The implication of these results is that it will be possible to obtain fluids with higher pvc characteristics by converting seed oil with low pvc into estolides. Higher pvc provides better lubrication in a number of applications including gear oils, bearing oils, motor oils, and metalworking fluids.

4. Summary/conclusion

Estolides are biobased oligo-esters obtained from the synthesis of ingredients derived from agricultural products. Estolides of varying purity, viscosity, and chemical structure were investigated and their film thickness and pressure–viscosity coefficient (pvc) characteristics compared to that of a commercial synthetic hydrocarbon, polyalpha olefin (PAO). Film-forming properties were investigated as a function of entrainment speed, at various temperatures and loads. The film thickness of estolides decreased with decreasing entrainment speed and increasing temperature, and was also independent of load. These results are similar to what has been

reported for other fluids, and demonstrates that estolides more or less follow the predictions of the EHL theory on the effect of measurement conditions on film thickness. Analysis of the film thickness data of estolides at high entrainment speeds showed that their film thickness follows the trend predicted by the Hamrock–Dowson equation (H–D). However, at low entrainment speeds, the measured film thickness of estolides displayed various degrees of deviations from that predicted by the H–D equation. These deviations were found to be functions of the purity and chemical structures of the estolides and not on their viscosities.

The pvc of estolides was calculated from their film thickness data using two different methods. The result shows that estolides have lower pvc than PAO, and their pvc were highly dependent on their purity and chemical structures. Estolides that were distilled to remove unreacted starting materials and side reaction products displayed higher pvc than those that were not purified. Also, a co-oligomer estolide gave a higher pvc than a homo-oligomer estolide, and this difference was attributed to the difference in the structures between these two purified estolides. The data also showed that, the pvc of a purified co-oligomer estolides was substantially higher than that reported for several seed oils. This comparison between estolides and seed oils is particularly interesting, since the fatty acids used in estolide synthesis are obtained from seed oils. The implication of the pvc results is that it will be possible to obtain biobased fluids with high pvc characteristics by converting the lower pvc seed oils into estolides.

Acknowledgments

The authors thank M. Goers for help with film thickness measurements; A. J. Thomas for dynamic viscosity measurements; A. Skender and A. Deppe for synthesis, purification, and characterization of estolides; BP Amoco for providing free sample of Durasyn 166; Prof. J. Wang and Dr. D. Zhu for reviewing and commenting on the manuscript.

References

- [1] D.L. Kaplan, in: *Biopolymers from Renewable Resources*, ed. D.L. Kaplan (Springer, Berlin, 1998), ch. 1.
- [2] R. Becker and A. Knorr, *Lubr. Sci.* 8 (1996) 95.
- [3] S.C. Cermak and T.A. Isbell, *J. Am. Oil Chem. Soc.* 78 (2001) 557.
- [4] T.A. Isbell, M.R. Edgecomb and B.A. Lowey, *Ind. Crops Prod.* 13 (2001) 11.
- [5] R.E. Harry-O'kuru, T.A. Isbell and D. Weisleder, *J. Am. Oil Chem. Soc.* 78 (2001) 219.
- [6] S.C. Cermak and T.A. Isbell, *Ind. Crops Prod.* 16 (2002) 119.
- [7] S.C. Cermak and T.A. Isbell, *Ind. Crops Prod.* 18 (2003) 183.
- [8] S.C. Cermak and T.A. Isbell, *Ind. Crops Prod.* 18 (2003) 223.
- [9] J.A. Schey, *Tribology in Metalworking Friction, Lubrication and Wear* (American Society of Metals, Metals Park, OH, 1983).
- [10] G. Biresaw, A. Adhvaryu, S.Z. Erhan and C.J. Carriere, *J. Am. Oil Chem. Soc.* 79(1)(2002) 53.
- [11] G. Biresaw, A. Adhvaryu and S.Z. Erhan, *J. Am. Oil Chem. Soc.* 80(2)(2003) 697.
- [12] G. Biresaw, *J. Am. Oil Chem. Soc.* 82(4)(2005) 285.
- [13] T.L. Kurth, G. Biresaw and A. Adhvaryu, *J. Am. Oil Chem. Soc.* 82(4)(2005) 293.
- [14] T.L. Kurth, S.C. Cermak, J.A. Byars and G. Biresaw, in: *Proceedings of World Tribology Congress III, 2005, WTC2005-64073* (Washington, DC, September 12–16, 2005).
- [15] T.A. Isbell and R. Kleiman, *J. Am. Oil Chem. Soc.* 71 (1994) 379.
- [16] G. Biresaw, *J. Am. Oil Chem. Soc.* 83(6)(2006) 559.
- [17] G.J. Johnston, R. Wayte and H.A. Spikes, *Tribology Trans.* 34 (1991) 187.
- [18] B.T. Hamrock and D. Dowson, *Ball Bearing Lubrication: The Elastohydrodynamics of Elliptical Surfaces* (Wiley, New York, 1981).
- [19] G. Guangteng and H.A. Spikes, *Wear* 200 (1996) 336.
- [20] G. Guangteng and H.A. Spikes, *Trib. Trans.* 40 (1997) 461.
- [21] H.A. Spikes, *Langmuir* 12 (1996) 4567.
- [22] H.A. Spikes, Plenary and Invited Papers from the World Tribology Congress, 1st, London, Sept. 8–12, 1997; (1997) 355.
- [23] H.A. Spikes, in: *Proceedings of the Royal Society–Unilever Indo-UK Forum in Materials Science and Engineering, 1st, London, Sept. 1994* (1996) 334.
- [24] S. Gunsel, S. Korcek, M. Smeeth and H.A. Spikes, *Trib. Trans.* 42 (1999) 559.